ACS APPLIED MATERIALS & INTERFACES

Research Article

www.acsami.org

Facile Synthesis of Electrospun $Li_{1.2}Ni_{0.17}Co_{0.17}Mn_{0.5}O_2$ Nanofiber and Its Enhanced High-Rate Performance for Lithium-Ion Battery Applications

Ji Won Min, Chul Jin Yim, and Won Bin Im*

School of Materials Science and Engineering, Chonnam National University, 300 Yongbong-dong, Buk-gu, Gwangju, 500-757, Republic of Korea

Supporting Information

ABSTRACT: The $Li_{1.2}Ni_{0.17}Co_{0.17}Mn_{0.5}O_2$ nanofibers were synthesized by a simple electrospinning process. Scanning electron microscopy (SEM) and transmission electron microscopy (TEM) showed that electrospun nanofibers with small particle size of 10−30 nm were formed. It was found that the electrospinning process leads to the formation of an effective conducting nanofiber, which provides improved intercalation kinetics. The eletrospun $Li_{1.2}Ni_{0.17}Co_{0.17}Mn_{0.5}O_2$ nanofibers showed a high discharge capacity of 256 mA h g^{-1} during the first cycle. In particular, the electrospun $Li_{1.2}Ni_{0.17}Co_{0.17}Mn_{0.5}O_2$ nanofiber sample exhibited excellent rate capability when compared to the co-precipitated $Li_{1.2}Ni_{0.17}Co_{0.17}Mn_{0.5}O_2$ particle sample.

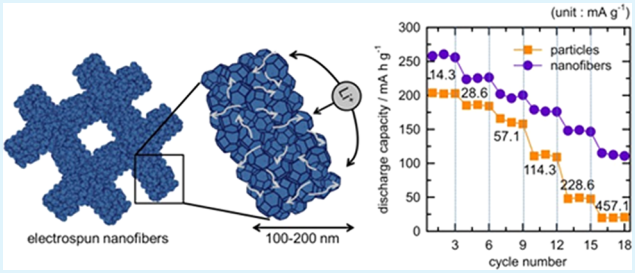

KEYWORDS: *lithium ion battery, cathode, layered−layered, electrospinning, nanofiber*

1. INTRODUCTION

As present, $LiCoO_2$ has been widely applied as one of the cathode materials in commercial lithium-ion batteries, due to its ease of production, stable electrochemical cycling, and acceptable specific capacity. The relatively high cost of cobalt and the lure of larger specific capacity have, however, led to the study of possible alternatives.[1] Recently, Li-rich cathode materials $xLi_2MnO_3\cdot(1-x)LiMO_2$ (M = Ni, Co, Mn, etc.) have attracted attention as cathode materials for high capacity of more than 250 mA h g^{-1}, with an operating voltage higher than 3.5 V vs Li/Li^{+1}.[2−4] The role of Li_2MnO_3, although it is electrochemically inactive up to 4.4 V, is also to contribute extra lithium to the reversible capacity (after its activation) and to facilitate lithium ion transport through the structure.[5]

However, Li-rich layered cathode materials are believed to have large irreversible capacity loss at first cycle and inherently low conductivity.[6−9] It is commonly accepted that the poor electrochemical performance of $xLi_2MnO_3\cdot(1-x)LiMO_2$ is associated with the oxygen loss from the surface[9] and insulating Li_2MnO_3 component, resulting in poor rate performance.[8] In order to overcome the afore mentioned demerits much effort has been made to enhance the rate capability of such cathode materials, like shortening the lithium ion diffusion pathways through reducing the particle size,[10−12] stabilizing the electrode/electrolyte interface by introducing an inert material,[13,14] and enhancing the electronic conductivity by coating a conductive surface layer.[15,16] Among these solutions, the preparation of nanostructure electrode has drawn increasing attention,[17] as these cathode materials are normally adopted to solve the kinetic problems associated with solid-state diffusion of lithium ion intercalation and electronic conductivity.[18]

In this paper, $Li_{1.2}Ni_{0.17}Co_{0.17}Mn_{0.5}O_2$ nanofibers were produced as cathode material for the first time by the combination of electrospinning and heat treatment. The physical, chemical, and electrochemical properties of the $Li_{1.2}Ni_{0.17}Co_{0.17}Mn_{0.5}O_2$ nanofibers were investigated by X-ray diffraction, field emission−scanning electron microscopy (FE-SEM), high resolution transmission electron microscopy (HR-TEM), Fourier transform infrared (FT-IR) spectroscopy, Brunauer, Emmett, and Teller (BET) measurements, and galvanostatic tests.

2. EXPERIMENTAL SECTION

2.1. Fabrication of $Li_{1.2}Ni_{0.17}Co_{0.17}Mn_{0.5}O_2$ Nanofiber. The solution for electrospinning was prepared from polyvinylpyrrolidone (PVP), *N*,*N*-dimethylformamide (DMF), lithium acetate dihydrate ($LiCH_3COO\cdot2H_2O$), manganese acetate ($Mn(CH_3COO)_2\cdot4H_2O$), nickel acetate ($Ni(CH_3COO)_2\cdot4H_2O$), and cobalt acetate ($Co(CH_3COO)_2\cdot4H_2O$). The mixture was stirred vigorously at room temperature for 24 h. A high voltage power supply (eS-robot®) was used to provide a high voltage at around 15−20 kV for electrospinning. Fibers were collected on an aluminum plate as a mat. Through those optimization processes, the nanofibers were calcined at 600°C for 12 h in air to eliminate the organic residues. The content of

Received: April 19, 2013
Accepted: August 1, 2013
Published: August 1, 2013

   dx.doi.org/10.1021/am402484f | ACS Appl. Mater. Interfaces 2013, 5, 7765−7769

carbon in the $Li_{1.2}Ni_{0.17}Co_{0.17}Mn_{0.5}O_2$ nanofiber sample was 0.28 wt %, as evaluated by CHN elemental analysis.

2.2. Preparation of $Li_{1.2}Ni_{0.17}Co_{0.17}Mn_{0.5}O_2$ Powders for Comparison. Li-excess transition metal oxides were synthesized using the co-precipitation process. Lithium hydroxide ($LiOH{\cdot}H_2O$), manganese acetate ($Mn(CH_3COO)_2{\cdot}4H_2O$), nickel acetate ($Ni(CH_3COO)_2{\cdot}4H_2O$), and cobalt acetate ($Co(CH_3COO)_2{\cdot}4H_2O$) were used, in appropriate mole fractions, to synthesize $Li_{1.2}Ni_{0.17}Co_{0.17}Mn_{0.5}O_2$. The precursor solutions were prepared by dissolving transition metal acetates and lithium hydroxide in distilled water and, after mixing together, were stirred for 24 h. The precipitated solutions were dried at 120 °C to evaporate water and annealed in air at 600 °C for 3 h. Subsequently, the powders were further heat treated at 900 °C for 12 h and quenched.

2.3. Structural and Physical Characterization. X-ray diffraction (XRD) data were obtained using Cu Kα radiation (Philips X'Pert) over the angular range $10° \leq 2\theta \leq 120°$, with a step size of 0.026°. The Rietveld refinement was made with the General Structure Analysis System (GSAS) program.[19] The particle morphologies and sizes were determined by field emission–scanning electron microscopy (FE-SEM) and high resolution transmission electron microscopy (HR-TEM). The SEM images were obtained using an S-4700 from Hitachi, and the TEM pictures were recorded using an FEI Tecnai F20 at 200 kV, in the Korea Basic Science Institute (KBSI). The BET method was used to measure the surface area of the powders. Fourier transform infrared (FT-IR) spectroscopy absorption spectra were recorded using an IRPresitge-21 from Shimadzu, at room temperature, in the spectral range 4000–400 cm^{-1}.

2.4. Electrochemical Characterization. The electrochemical properties of $Li_{1.2}Ni_{0.17}Co_{0.17}Mn_{0.5}O_2$ were evaluated, with lithium metal as the reference electrode. For the electrochemical measurements, a mass ratio of 75:10:15 of active material, conductive carbon (KETJEN black), and PTFE binder, respectively, was used for the electrode fabrication. This mixture was pressed onto a stainless steel mesh and dried under vacuum at 120 °C for 12 h. A 2032 coin type cell, consisting of cathode and lithium metal anode separated by a polymer membrane together with glass fiber, was fabricated in an Ar-filled glovebox and aged for 12 h, before the electrochemical measurements. The electrolyte was a 1:1 mixture of ethylene carbonate (EC) and dimethyl-carbonate (DMC) containing 1 M $LiPF_6$.

3. RESULTS AND DISCUSSION

3.1. Morphology and Structure Characterization. The morphology of the products was examined by scanning electron microscopy (SEM). The $Li_{1.2}Ni_{0.17}Co_{0.17}Mn_{0.5}O_2$ sample prepared by the co-precipitation indicates the aggregation of small particles of size around 100–200 nm and irregular shapes, as in Figures 1a,b. The $Li_{1.2}Ni_{0.17}Co_{0.17}Mn_{0.5}O_2$ sample prepared by electrospinning showed that the diameters of the nanofibers were mainly around 100–200 nm, with minimum of less than 80 nm, as shown in Figures 1c,d. This is clearly linked to the considerable difference in the BET values of 2.824 m^2 g^{-1} for nanopowder of $Li_{1.2}Ni_{0.17}Co_{0.17}Mn_{0.5}O_2$ sample prepared by co-precipitation and 17.849 m^2 g^{-1} for nanofiber of $Li_{1.2}Ni_{0.17}Co_{0.17}Mn_{0.5}O_2$ sample prepared by electrospinning. Such morphology of the nanofibers is expected to facilitate electrolyte penetration into the electrode particles, thus providing more interface area between the electrode material and the electrolyte.[20,21]

Figure 1e,f shows TEM images of $Li_{1.2}Ni_{0.17}Co_{0.17}Mn_{0.5}O_2$ nanofibers. Results confirm that $Li_{1.2}Ni_{0.17}Co_{0.17}Mn_{0.5}O_2$ nanoparticles are dispersed inside the nanofiber matrix (Figure 1f). As shown in Figure 1e, some $Li_{1.2}Ni_{0.17}Co_{0.17}Mn_{0.5}O_2$ nanoparticles aggregate to form clusters, but they are still smaller than 30 nm. It implied that these $Li_{1.2}Ni_{0.17}Co_{0.17}Mn_{0.5}O_2$ nanofibers were composed of individual crystallites. As shown in Figure 1f, lattice planes were observed as clear in $Li_{1.2}Ni_{0.17}Co_{0.17}Mn_{0.5}O_2$, indicating the well crystalline structure. These results were consistent with XRD analysis. Figure 2 shows schematic diagrams of the electron transfer pathway of the electrospun $Li_{1.2}Ni_{0.17}Co_{0.17}Mn_{0.5}O_2$ nanofiber.

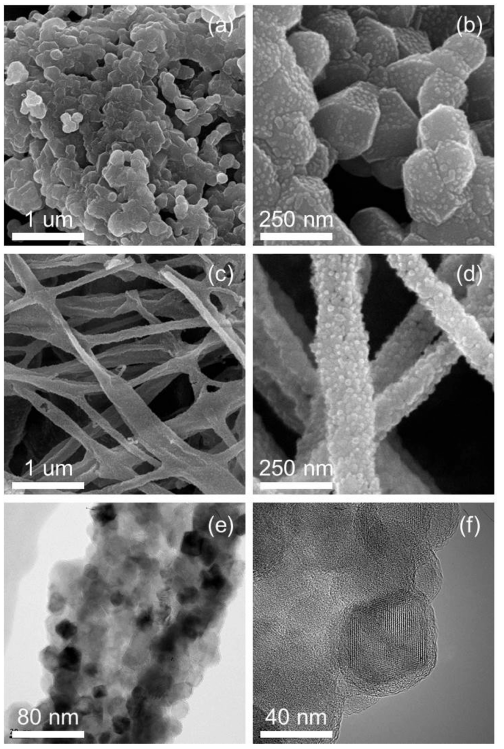

Figure 1. SEM images of (a and b) $Li_{1.2}Ni_{0.17}Co_{0.17}Mn_{0.5}O_2$ particles and (c and d) $Li_{1.2}Ni_{0.17}Co_{0.17}Mn_{0.5}O_2$ nanofibers and TEM images of (e and f) $Li_{1.2}Ni_{0.17}Co_{0.17}Mn_{0.5}O_2$ nanofibers.

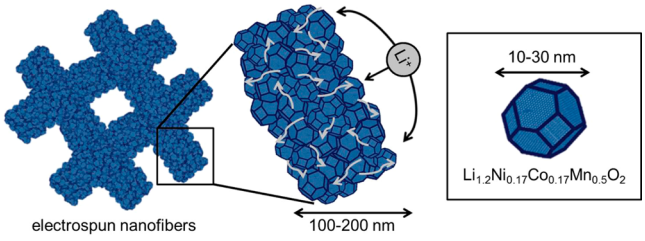

Figure 2. Schematic diagrams of the electron transfer pathway of the $Li_{1.2}Ni_{0.17}Co_{0.17}Mn_{0.5}O_2$ nanofiber by electrospinning.

Figure 3 shows the LeBail fitting results of the XRD profiles of co-precipitated and electrospun $Li_{1.2}Ni_{0.17}Co_{0.17}Mn_{0.5}O_2$ samples, respectively. On the basis of the LeBail fitting results, the initial structural models, which approximate the actual structures of $Li_{1.2}Ni_{0.17}Co_{0.17}Mn_{0.5}O_2$, were constructed with the crystallographic data previously reported.[22] The results confirmed the single-phase nature of the compounds in the α-$NaFeO_2$-type structure ($R\bar{3}m$). However, small extra peaks around 20–23° in the XRD profiles are generally attributed to the ordering of Li and Mn in the transition-metal layers, which can be indexed to the Li_2MnO_3 system.[5] Table 1 lists the fitted structural parameters and structural information.

3.2. FT-IR Analysis. The $Li_{1.2}Ni_{0.17}Co_{0.17}Mn_{0.5}O_2$ samples underwent Fourier transform infrared (FT-IR) spectroscopy analysis to examine the effect of the nature of the PVP

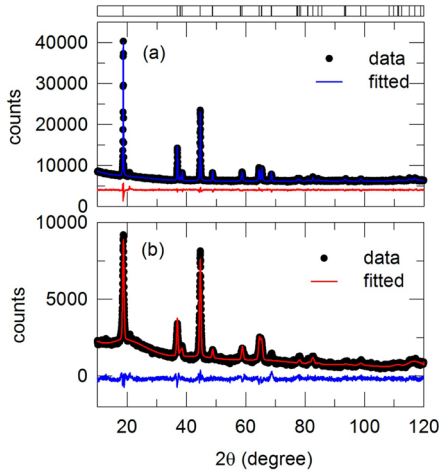

Figure 3. LeBail fitting results of the powder X-ray diffraction profile of (a) co-precipitated and (b) electrospun $Li_{1.2}Ni_{0.17}Co_{0.17}Mn_{0.5}O_2$. Data (points) and fit (lines) show the different profile XRD patterns of the $Li_{1.2}Ni_{0.17}Co_{0.17}Mn_{0.5}O_2$. Expected reflection positions for the $Li_{1.2}Ni_{0.17}Co_{0.17}Mn_{0.5}O_2$ are displayed at the top.

Table 1. LeBail Fitting Results and Crystal Data for $Li_{1.2}Ni_{0.17}Co_{0.17}Mn_{0.5}O_2$ by X-ray Diffraction[a]

	coprecipitation	electronspun
radiation type	Cu Kα	
2θ range (degree)	10−120	
T, K	295	
symmetry	trigonal	
space group	$R\bar{3}m$	
a, Å	2.853(2)	2.854(1)
c, Å	14.249(2)	14.214(2)
volume, Å^3	100.5(1)	100.3(1)
Z	3	3
R_{wp}	4.13%	2.64%
χ^2	1.950	1.491

[a]The numbers in parentheses are the estimated standard deviations of the last significant figure.

participating in the chemical reactions. The FT-IR adsorption band for the metal−oxygen (M−O) of $Li_{1.2}Ni_{0.17}Co_{0.17}Mn_{0.5}O_2$ appears in the wavenumber range of 500−700 cm^{-1}, indicating the formation of inorganic targets.[23] The peaks of $Li_{1.2}Ni_{0.17}Co_{0.17}Mn_{0.5}O_2$ particles appear at 621.1 and 530.4 cm^{-1}, and those of $Li_{1.2}Ni_{0.17}Co_{0.17}Mn_{0.5}O_2$ nanofiber appear at 621.1 and 538.1 cm^{-1}, as shown in Figure 4. The characteristic peaks of $Li_{1.2}Ni_{0.17}Co_{0.17}Mn_{0.5}O_2$ nanofiber at 500−700 cm^{-1} were smoother than those of $Li_{1.2}Ni_{0.17}Co_{0.17}Mn_{0.5}O_2$ particles, indicating that the decomposition of PVP leads to poor crystallinity of the compound.[24,25] These results are in accordance with the lower intensity of the $Li_{1.2}Ni_{0.17}Co_{0.17}Mn_{0.5}O_2$ peak in the XRD pattern.

3.3. Electrochemical Performance. To evaluate the electrochemical performance of the $Li_{1.2}Ni_{0.17}Co_{0.17}Mn_{0.5}O_2$ sample, charge−discharge cycles were conducted at room temperature, between 2.0 and 4.8 V at a current density of 14.3 mA g^{-1}, and the results are shown in Figure 5. The $Li_{1.2}Ni_{0.17}Co_{0.17}Mn_{0.5}O_2$ nanofibers delivered a charge capacity as high as 331 mA h g^{-1} above 4.5 V and a discharge capacity of 256 mA h g^{-1}, while those of the $Li_{1.2}Ni_{0.17}Co_{0.17}Mn_{0.5}O_2$ particles were observed to be 269 and 193 mA h g^{-1}. The nanofiber electrode has higher capacity than the nanoparticle

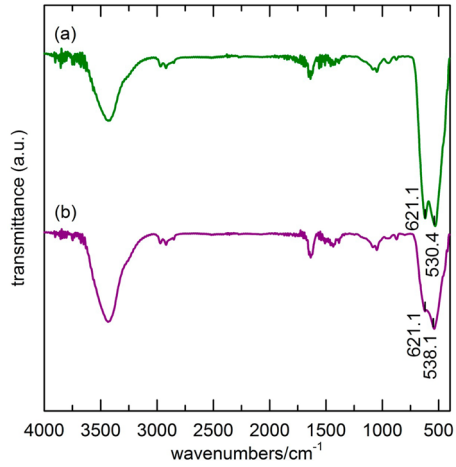

Figure 4. FT-IR spectra of (a) $Li_{1.2}Ni_{0.17}Co_{0.17}Mn_{0.5}O_2$ particles and (b) $Li_{1.2}Ni_{0.17}Co_{0.17}Mn_{0.5}O_2$ nanofibers.

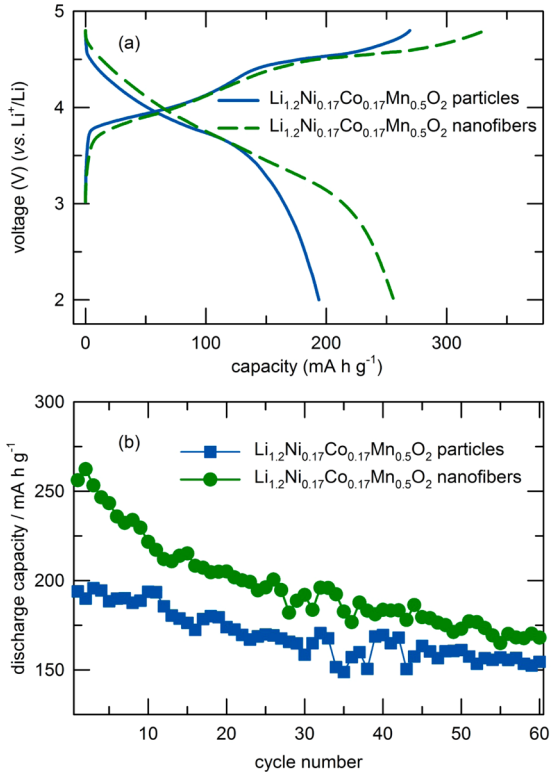

Figure 5. (a) Voltage profiles of the samples obtained for the first cycle and (b) cyclabilities in the voltage range of 2.0−4.8 V, at a current density of 14.3 mA g^{-1}.

electrode. The large capacity of $Li_{1.2}Ni_{0.17}Co_{0.17}Mn_{0.5}O_2$ nanofibers electrode at first cycle is attributed to large surface area. With high surface-to-volume ratios, the nanofiber structure allows more contact between the electrode and electrolyte.[26] Figure 5b presents the capacity retention of the $Li_{1.2}Ni_{0.17}Co_{0.17}Mn_{0.5}O_2$ sample, at current density of 14.3 mA g^{-1}. The capacity retentions of $Li_{1.2}Ni_{0.17}Co_{0.17}Mn_{0.5}O_2$ nanofibers were 66% and those of particles were 79% at the 60th cycle. The poor capacity retention of Li/$Li_{1.2}Ni_{0.17}Co_{0.17}Mn_{0.5}O_2$ nanofibers is probably due to its poor crystallinity. These results are in accordance with our XRD and FT-IR data. However, from the 10th cycle to 60th cycle, the capacity retentions of $Li_{1.2}Ni_{0.17}Co_{0.17}Mn_{0.5}O_2$ nanofibers were

dx.doi.org/10.1021/am402484f | ACS Appl. Mater. Interfaces 2013, 5, 7765−7769

76%. Although from first cycle the $Li_{1.2}Ni_{0.17}Co_{0.17}Mn_{0.5}O_2$ nanofibers showed poor capacity retention, they showed better capacity retention as the number of cycles increased.

Finally, the rate-performance of the electrodes was tested, using different current densities. Figure 6 shows variations in discharge capacities versus charge−discharge cycle number, for different $Li_{1.2}Ni_{0.17}Co_{0.17}Mn_{0.5}O_2$ electrodes cycled at different rates, between 2.0 and 4.8 V at room temperature. The cells were charged using a current density of 14.3 mA g^{-1}, before each discharge test. The discharge capacity of the $Li_{1.2}Ni_{0.17}Co_{0.17}Mn_{0.5}O_2$ particles decreases with increasing current density when cycled between 2.0 and 4.8 V,and reaches 23 and 9% at 228.6 and 457.1 mA g^{-1}, compared with the specific capacity of 203 mA h g^{-1} at 14.3 mA g^{-1}, respectively. On the other hand, the discharge capacity of the $Li_{1.2}Ni_{0.17}Co_{0.17}Mn_{0.5}O_2$ nanofibers cathode material decreases to a smaller extent with increasing current density, when cycled between 2.8 and 4.8 V, and reaches 57 and 43% at 228.6 and 457.1 mA g^{-1}, compared with the capacity of 266 mA h g^{-1} at 14.3 mA g^{-1}, respectively. This behavior shows that the rate capability of $Li_{1.2}Ni_{0.17}Co_{0.17}Mn_{0.5}O_2$ was significantly improved by the electrospinning method.

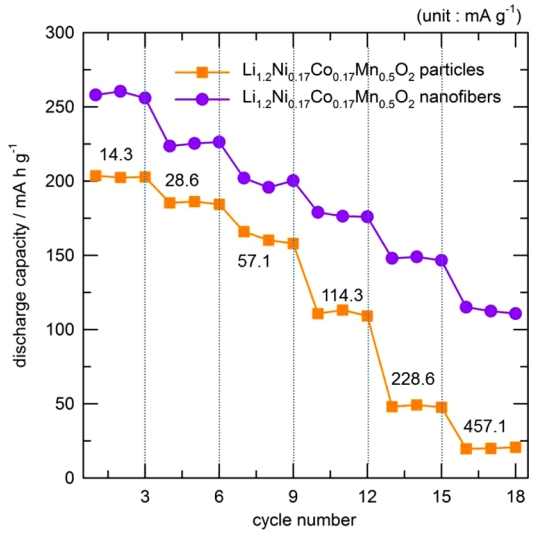

Figure 6. Rate capabilities of $Li_{1.2}Ni_{0.17}Co_{0.17}Mn_{0.5}O_2$ particles and $Li_{1.2}Ni_{0.17}Co_{0.17}Mn_{0.5}O_2$ nanofibers, cycled between 2.0 and 4.8 V. The cell was charged using a specific current of 14.3 mA g^{-1}, before each discharge test.

Many researchers highlighted the role of carbon coating and morphology on the electrochemical performance of electrospun nanofiber materials.[27−29] In order to determine the factors affecting the electrochemical properties of electrospun $Li_{1.2}Ni_{0.17}Co_{0.17}Mn_{0.5}O_2$ nanofiber, we analyzed the presence of carbon in our $Li_{1.2}Ni_{0.17}Co_{0.17}Mn_{0.5}O_2$ nanofiber by Raman study. Figure S1 (see Supporting Information) shows the Raman spectrum of $Li_{1.2}Ni_{0.17}Co_{0.17}Mn_{0.5}O_2$ nanofiber material. It is notable that this material contains no significant carbon in Raman analysis, even though we used polymer precursors for synthesis. The PVP polymer decomposes around 430 °C while heat treated at 600 °C in air and is shown in the TGA/DSC result (Figure S2, Supporting Information). These results were consistent with CHN elemental analysis. This may be the reason for the absence of carbon in the electrospun $Li_{1.2}Ni_{0.17}Co_{0.17}Mn_{0.5}O_2$ nanofiber. In this regard, we believe that the outstanding performance of electrospun $Li_{1.2}Ni_{0.17}Co_{0.17}Mn_{0.5}O_2$ nanofiber at high current rate can be understood in terms of morphological features. A key factor for the limitation in rate capability is due to the difficult solid state diffusion of Li ion. The electrospun $Li_{1.2}Ni_{0.17}Co_{0.17}Mn_{0.5}O_2$ nanofiber with small particle size of 10−30 nm might be used to reduce the diffusion distance of Li ion in the solid state.[30] In addition, an effective conducting nanofiber improves the electrical contact between the cathode particles and results in improved intercalation kinetics.

4. CONCLUSIONS

$Li_{1.2}Ni_{0.17}Co_{0.17}Mn_{0.5}O_2$ nanofibers were synthesized via a simple electrospinning process. Their crystal structure, morphology characteristics, and electrochemical performance were thoroughly investigated. The electrospun nanofibers with small particle size of 10−30 nm provided fast lithium ion intercalation and de-intercalation properties, leading to an enhanced rate capability for $Li_{1.2}Ni_{0.17}Co_{0.17}Mn_{0.5}O_2$ nanofibers. The simple synthesis method may be applicable to commercialization of the Li-rich layered cathode materials, which could be applied in Plug-in Hybrid Electric Vehicle (PHEV) and Electric Vehicle (EV).

■ ASSOCIATED CONTENT

Ⓢ Supporting Information

Raman spectra, TGA, and DSC. This material is available free of charge via the Internet at http://pubs.acs.org.

■ AUTHOR INFORMATION

Corresponding Author

*Tel.: +82-62-530-1715. Fax: +82-62-530-1699. E-mail: imwonbin@jnu.ac.kr.

Notes

The authors declare no competing financial interest.

■ ACKNOWLEDGMENTS

This research was supported by the MSIP (Ministry of Science, ICT & Future Planning), Korea, under the C-ITRC (Convergence Information Technology Research Center) support program (NIPA-2013-H0301-13-1009) supervised by the NIPA (National IT Industry Promotion Agency). This research is also supported by Ministry of Education, Science Technology (MEST) and National Research Foundation of Korea (NRF) through the Human Resource Training Project for Regional Innovation.

■ REFERENCES

(1) Li, H.; Wang, Z. X.; Chen, L. Q.; Huang, X. J. *Adv. Mater.* **2009**, *21*, 4593−4607.
(2) Lu, Z. H.; MacNeil, D. D.; Dahn, J. R. *Electrochem. Solid State Lett.* **2001**, *4*, A191−A194.
(3) Kim, J. S.; Johnson, C. S.; Vaughey, J. T.; Thackeray, M. M.; Hackney, S. A. *Chem. Mater.* **2004**, *16*, 1996−2006.
(4) Thackeray, M. M.; Johnson, C. S.; Vaughey, J. T.; Li, N.; Hackney, S. A. *J. Mater. Chem.* **2005**, *15*, 2257−2267.
(5) Thackeray, M. M.; Kang, S. H.; Johnson, C. S.; Vaughey, J. T.; Benedek, R.; Hackney, S. A. *J. Mater. Chem.* **2007**, *17*, 3112−3125.
(6) Kang, S. H.; Johnson, C. S.; Vaughey, J. T.; Amine, K.; Thackeray, M. M. *J. Electrochem. Soc.* **2006**, *153*, A1186−A1192.
(7) Deng, Z. Q.; Manthiram, A. *J. Phys. Chem. C* **2011**, *115*, 7097−7103.

(8) Kang, S. H.; Kempgens, P.; Greenbaum, S.; Kropf, A. J.; Amine, K.; Thackeray, M. M. *J. Mater. Chem.* **2007**, *17*, 2069−2077.
(9) Armstrong, A. R.; Holzapfel, M.; Novak, P.; Johnson, C. S.; Kang, S. H.; Thackeray, M. M.; Bruce, P. G. *J. Am. Chem. Soc.* **2006**, *128*, 8694−8698.
(10) Wei, G. Z.; Lu, X.; Ke, F. S.; Huang, L.; Li, J. T.; Wang, Z. X.; Zhou, Z. Y.; Sun, S. G. *Adv. Mater.* **2010**, *22*, 4364−4367.
(11) Kim, M. G.; Jo, M.; Hong, Y. S.; Cho, J. *Chem. Commun.* **2009**, 218−220.
(12) Cho, J.; Kim, Y.; Kim, M. G. *J. Phys. Chem. C* **2007**, *111*, 3192−3196.
(13) Sun, Y. K.; Lee, M. J.; Yoon, C. S.; Hassoun, J.; Amine, K.; Scrosati, B. *Adv. Mater.* **2012**, *24*, 1192−1196.
(14) Liu, J.; Manthiram, A. *J. Mater. Chem.* **2010**, *20*, 3961−3967.
(15) Liu, J.; Wang, Q. Y.; Reeja-Jayan, B.; Manthiram, A. *Electrochem. Commun.* **2010**, *12*, 750−753.
(16) Martha, S. K.; Nanda, J.; Veith, G. M.; Dudney, N. J. *J. Power Sources* **2012**, *216*, 179−186.
(17) Cheng, F. Q.; Xin, Y. L.; Chen, J. T.; Lu, L.; Zhang, X. X.; Zhou, H. H. *J. Mater. Chem. A* **2013**, *1*, 5301−5308.
(18) Zhang, S. C.; Qiu, X. P.; He, Z. Q.; Weng, D. S.; Zhu, W. T. *J. Power Sources* **2006**, *153*, 350−353.
(19) Larson, A. C.; Von Dreele, R. B. *General Structure Analysis System (GSAS)*; Los Alamos National Laboratory Report LAUR 86-748; Los Alamos National Laboratory: 1994.
(20) Sun, C. W.; Rajasekhara, S.; Goodenough, J. B.; Zhou, F. *J. Am. Chem. Soc.* **2011**, *133*, 2132−2135.
(21) Ou, Y.; Wen, J. J.; Xu, H. P.; Xie, S. H.; Li, J. Y. *J. Phys. Chem. Solids* **2013**, *74*, 322−327.
(22) Tran, N.; Croguennec, L.; Menetrier, M.; Weill, F.; Biensan, P.; Jordy, C.; Delmas, C. *Chem. Mater.* **2008**, *20*, 4815−4825.
(23) Pavia, D. L. *Introduction to spectroscopy*, 4th ed.; Cengage Learning: 2009.
(24) Song, C. H.; Stephan, A. M.; Jeong, S. K.; Hwang, Y. J.; Kim, A. R.; Nahm, K. S. *J. Electrochem. Soc.* **2006**, *153*, A390−A395.
(25) Shao, C. L.; Yu, N.; Liu, Y. C.; Mu, R. X. *J. Phys. Chem. Solids* **2006**, *67*, 1423−1426.
(26) Zhang, X.; Xing, Z.; Yu, Y.; Li, Q. W.; Tang, K. B.; Huang, T.; Zhu, Y. C.; Qian, Y. T.; Chen, D. *CrystEngComm* **2012**, *14*, 1485−1489.
(27) Zhang, S.; Lin, Z.; Ji, L. W.; Li, Y.; Xu, G. J.; Xue, L. G.; Li, S. L.; Lu, Y.; Toprakci, O.; Zhang, X. W. *J. Mater. Chem.* **2012**, *22*, 14661−14666.
(28) Zhang, S.; Li, Y.; Xu, G.; Li, S.; Lu, Y.; Toprakci, O.; Zhang, X. *J. Power Sources* **2012**, *213*, 10−15.
(29) Toprakci, O.; Toprakci, H. A. K.; Ji, L.; Xu, G.; Lin, Z.; Zhang, X. *ACS Appl. Mater. Interface* **2012**, *4*, 1273−1280.
(30) Ding, Y.; Zhang, P.; Long, Z.; Jiang, Y.; Gao, D. *J. Alloys Compd.* **2008**, *462*, 340−342.